# Hydrodynamic performance of a self-propelled KCS at angle of drift including rudder forces

**Yifu Zhang[*], Björn Windén[†‡], Dominic Hudson[*], Stephen Turnock[*]**
*Maritime Engineering, University of Southampton, UK
†SHORTCUt CFD LLC, College Station, Texas, USA
‡Texas A&M University, College Station, Texas, USA
Corresponding email: yz26g15@soton.ac.uk

## 1 Introduction

Accurate prediction of ship manoeuvring in a seaway is one of the most critical requirements in ship design and its operation. This is especially true when a ship sails in adverse weather. However, the understanding of ship manoeuvrability in real sea states is not well developed (ITTC, 2021). Manoeuvring prediction capability is still challenging compared with resistance, propulsion and seakeeping (Sanada et al. 2021). Traditional experimental approaches for evaluating ship manoeuvring performance include free-running model tests and captive model tests in a towing tank or wave basin. Free-running model tests assess the manoeuvring characteristics directly by conducting prescribed turning or zigzag test. In comparison, captive tests are conducted to generate hydrodynamic force/moment derivatives (manouevring coefficients) and then use simulations of ship free-running tests by solving ship motion equations where the forces and moments are approximated by using the obtained hydrodynamic derivatives (Jiang et al., 2022). Although conventional model test can provide accurate and reliable maneuvering calculations, it is still costly and has a high specification for the ship model and test facilities. Benefiting from the rapid development of high performance computing, numerical methods are able to offer potentially a more cost-effective approach to determine the ship manoeuvring performance with more detail of hull-appendages interaction in stern region, which is less likely to be observed in towing tank tests.

To predict performance of a ship during a manoeuvre, the accurate determination of rudder forces when sailing at an angle of drift is necessary. The interaction between the forces and moments generated on the hull and propeller upstream of the rudder has strong influence on rudder forces (Badoe et al., 2015). In this paper, the hull-propeller-rudder interaction of the benchmark KRISO Container Ship (KCS) in calm water is studied using Computational Fluid Dynamics (CFD). The self-propelled KCS is simulated at static drift angles combined with a series of rudder angles, which represents quasi-static phases of an actual ship manoeuvre. This innovative approach removes the need for modelling the complete time varying manoeuvre, which greatly reduces the computational cost and provides reference for experimental calculations of hull and appendage forces when the angle of drift is applied (Zhang et al., 2021). The results and analysis of the effect of static drift angles and rudder angles on resistance, side force, yaw moment, and propulsive performance will be demonstrated.

## 2 Methodology

The fluid flow around the KCS is modelled using the Reynolds Averaged Navier-Stokes (RANS) equations with the assumption of an incompressible fluid (Zhang et al., 2021). For all calculations in this paper, the basic incompressible solver of OpenFOAM v.7 (OpenFOAMFoundation, 2019), simpleFoam, is adopted for pressure-velocity coupling to achieve the resistance tests. simpleFoam is also coupled with a body force propeller model, using Blade Element Momentum Theory (BEMt), to compute the self-propulsion tests.

The choice of using a body force model for propeller modelling aims to reduce the computational cost in self-propulsion simulations. A body force model does not discretize the actual geometry of the propeller; and therefore, the total mesh size is reduced significantly. For body force methods, the momentum yielded by the propeller blades is directly added to the RANS momentum equation as an

extra momentum source (or body force.) Expressing the RANS momentum equations in Cartesian coordinates, the flow field $\bar{u} = (u, v, w)$ is accelerated by the body force $\overline{F_{\bar{v}}} = (F_{vx}, F_{vy}, F_{vz})$. The momentum equations with body force term can be written in the form:

$$\frac{\partial(\rho \mathrm{u})}{\partial \mathrm{t}} + \nabla \cdot (\rho u \bar{u}) = -\frac{\partial \mathrm{p}}{\partial \mathrm{x}} + \frac{\partial \tau_{xx}}{\partial \mathrm{x}} + \frac{\partial \tau_{yx}}{\partial \mathrm{y}} + \frac{\partial \tau_{zx}}{\partial \mathrm{z}} + \rho F_{vx} \quad (1)$$

$$\frac{\partial(\rho \mathrm{v})}{\partial \mathrm{t}} + \nabla \cdot (\rho v \bar{u}) = -\frac{\partial \mathrm{p}}{\partial \mathrm{y}} + \frac{\partial \tau_{xy}}{\partial \mathrm{x}} + \frac{\partial \tau_{yy}}{\partial \mathrm{y}} + \frac{\partial \tau_{zy}}{\partial \mathrm{z}} + \rho F_{vy} \quad (2)$$

$$\frac{\partial(\rho \mathrm{w})}{\partial \mathrm{t}} + \nabla \cdot (\rho w \bar{u}) = -\frac{\partial \mathrm{p}}{\partial \mathrm{z}} + \frac{\partial \tau_{xz}}{\partial \mathrm{x}} + \frac{\partial \tau_{yz}}{\partial \mathrm{y}} + \frac{\partial \tau_{zz}}{\partial \mathrm{z}} + \rho F_{vz} \quad (3)$$

To compute the body force $\overline{F_{\bar{v}}}$ distribution, there are numerous approaches with different levels of complexity, such as an actuator disc where the force is spread over the radius and a full panel method where the force is derived from each panel's pressure etc (Windén, 2021).

In this paper, BEMt is adopted for propeller modelling in all cases. BEMt combines 2D blade element theory and momentum theory. The combination of these two methods eliminates some difficulties of calculating the induced velocity of the propeller. The implementation of the BEMt follows the procedure by Molland et al. (2017). The advantage of BEMt over more advanced methods is a much lower computational cost as well as the capability of tuning the lift and drag properties of the 2D blade sections to the local Reynolds number. BEMt also allows for inclusion of viscous effects such as stall and the effect of laminar separation at low Reynolds number (Phillips et al., 2009). The coupling of RANS and BEMt has been successfully achieved in investigating ship hydrodynamic performance and fluid-structure interactions (Phillips et al., 2010; Windén, 2014; Badoe, 2015; Zhang et al., 2021). Furthermore, BEMt is an accurate and cost-effective approach for predicting URANS simulations of static drift and dynamic maneuvers of self-propelled KVLCC2 tanker (Turnock et al., 2008).

## 3 Computational implementations

### Vessel choice and its particulars

The KRISO Container Ship (KCS) is chosen as the ship model in this study as it has been widely studied experimentally and computationally and it provides detailed insights for both explanations of flow physics and numerical validation and verification for a modern container ship. Table 1 shows the main particulars of the KCS, including propeller and rudder.

*Table 1. Main Particulars of studied KCS.*

| Property | Model Scale | Full Scale |
|---|---|---|
| Lpp (m) | 7.2786 | 230 |
| Fn | 0.26 | 0.26 |
| U(m/s, full scale knots) | 2.196 | 24 |
| S w/o rudder (m^2) | 9.4379 | 9424 |
| Propeller | | |
| Diameter (m) | 0.25 | 7.9 |
| No. Blades | 5 | |
| Rotation Direction | Clockwise | |
| Rudder | | |
| Type | semi-balanced horn rudder | |
| S of rudder (m^2) | 0.1152 | 115 |
| Lat. Area (m^2) | 0.545 | 54.45 |

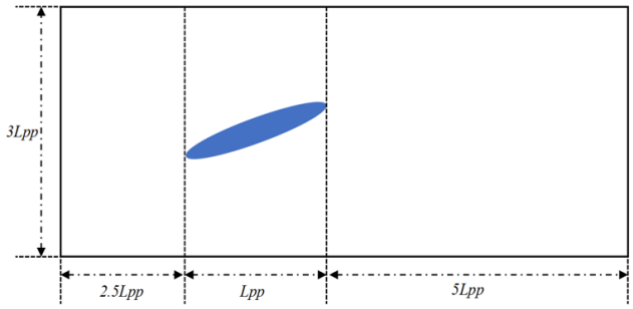


*Figure 1. Dimensions of domain. The depth of domain is 1.5Lpp.*

### Computational domain and mesh

With the use of SHORTCUt open source framework (Windén, 2021), the size of computational domain is scaled to the same dimensions relative to the Lpp of KCS. The dimensions of domain are presented in Figure 1. SHORTCUt uses the OpenFOAM utilities blockMesh and the unstructured mesher snappyHexMesh and it has six main refinement zones: 1)The background mesh (freestream); 2)A box enclosing the whole hull; 3)Smaller boxes extending forward/aft of, and enclosing the bow/stern region;

4)Cylinder extending forward/aft of, and enclosing the propeller; 5)Surface refinement on hull and rudder; 6)Prism layer inside the boundary layer on hull and rudder. The detailed explanation of these six refinement zones are presented in Windén, 2021.

**Calculated cases and solvers**

The KCS model with rudder is simulated using a double model setup: no above-water geometry is included, and the dynamics of the free surface is not modelled. Two different values of drift angle are chosen: 0° and 7.5° respectively. Seven different rudder angles are applied to every drift case: -10°, -7.5°, -5°, 0°, 5°, 7.5° and 10°. In all cases, the RANS equations are solved in iterative way using the SIMPLE algorithm. For each case, the first 1000 iterations are conducted for the hull with rudder (resistance test) using the simpleFoam solver. This computes the towed resistance of the hull with rudder, and it can provide a reference to find the ship self-propulsion point. The resistance test also initializes the flow field for the following self-propulsion test using the custom solver selfPropsimpleFoam. Another 1000 iterations are then conducted with the BEMt propeller model switched on. This yields self-propelled KCS's resistance, thrust and torque. In addition, three sets of fixed RPM tests are conducted for all cases.

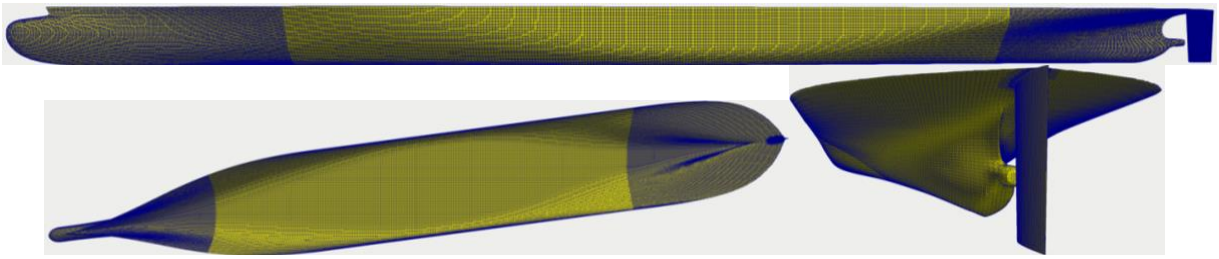

*Figure 2. Mesh of 7.5° drifted KCS with 0° rudder after snappyHexMesh (side, top, rear views)*

## 4 Results and discussion

**Resistance, side force and yaw moment**

As shown in Figure 3 (a), when there is no drift angle applied, the total resistance of the hull with rudder increases with the increment of rudder angle. $C_T$ lines of resistance and self-propulsion are almost axisymmetric around $\beta_r$=0°. In comparison, when the rudder angle is increased from -10° to +10°, the total resistance has a continuously increasing trend when the drift angle is 7.5°. The increment in $C_T$ is more obvious in self-propulsion tests, when compared with resistance tests in the two drifted scenarios. The resistance distribution of different fixed RPM values is presented in Figure 3 (f) and the values of fixed RPM chosen as 1900, 2400 and 3000 since RPM=1900, 2400 are close to the RPM values for the self-propulsion point when drift angle is 0°and 7.5° respectively and RPM=3000 represents a 25% increment over RPM=2400. The overall trend is that $C_T$ increases when the value of RPM increases for both drift angles. When the drift angle is 0°, the resistance for +$\beta_r$ and -$\beta_r$ is similar, which is similar to the trend in Figure 3 (a). For cases of 7.5° drift, the increment of resistance is more significant when the rudder angle varies from -10° to +10°. $C_T$ at $\beta_r$=10° is approximately 1.45 times of that at $\beta_r$=-10° when RPM=3000. Therefore, it is concluded that the influence of rudder angle on $C_T$ is more evident when a non-zero drift angle is applied.

Side force and yaw moment on the hull and the rudder are computed with all values non-dimensionalized using Equation (4). Variations in the hull side force and yaw moment are found to be almost linear with rudder angle varying from -10° to 10° for both drifted cases as shown in Figure 3 (b) and (c). When the drift is 0°, the hull side force and yaw moment plots of coincide with each other for both the resistance and self-propulsion. In 7.5° drift cases, the hull $F_Y'$ in the self-propulsion test is slightly larger than that of the resistance test while the hull $M_Z'$ in the self-propulsion test is lower than that of the pure resistance test for the corresponding rudder angles. In comparison, the overall variation trend of the rudder side force and yaw moment is the same. This is presented in Figure 3 (d) and (e).

The plots of side force and yaw moment are axisymmetric around $\beta_r$=0° when there is no drift angle applied. For 7.5° drifted cases, the variation slope with rudder angle for the side force and yaw moment is steeper than for the zero drift cases.

$$F_Y' = \frac{f_y(N)}{\rho \times U^2 \times L_{pp}^2} \quad and \quad M_Z' = \frac{m_z}{\rho \times U^2 \times L_{pp}^3} \tag{4}$$

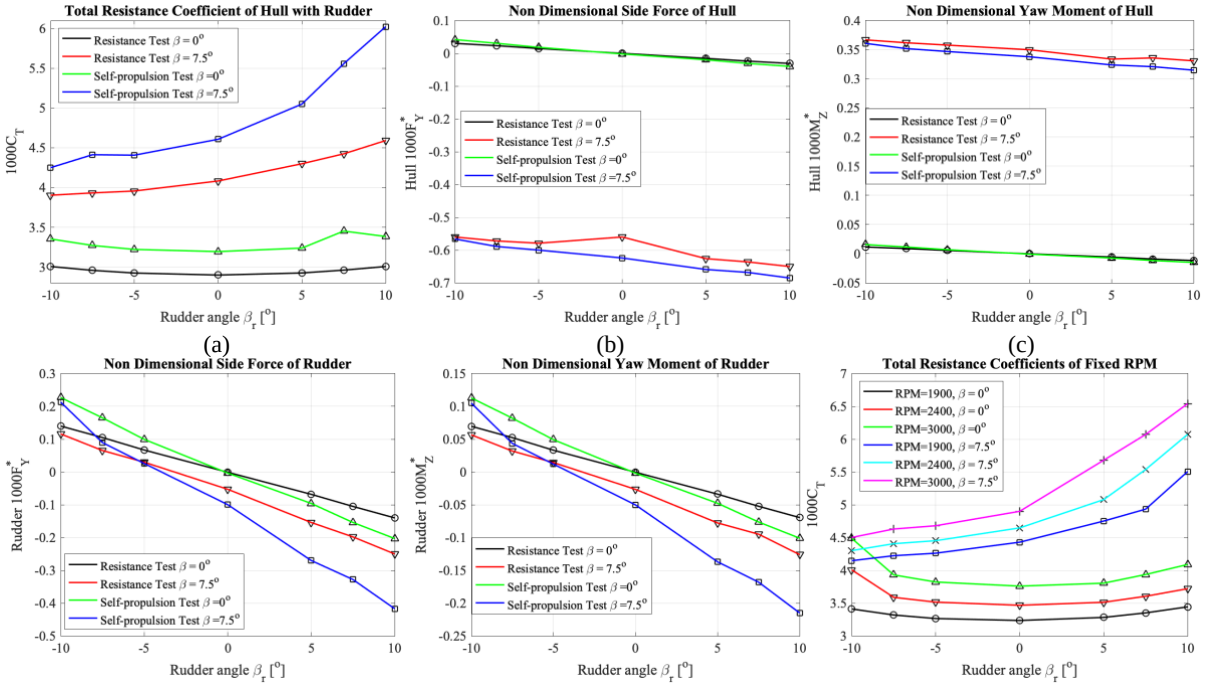


*Figure 3. Influence of drift angle on resistance and side force, yaw moment of hull and rudder.*

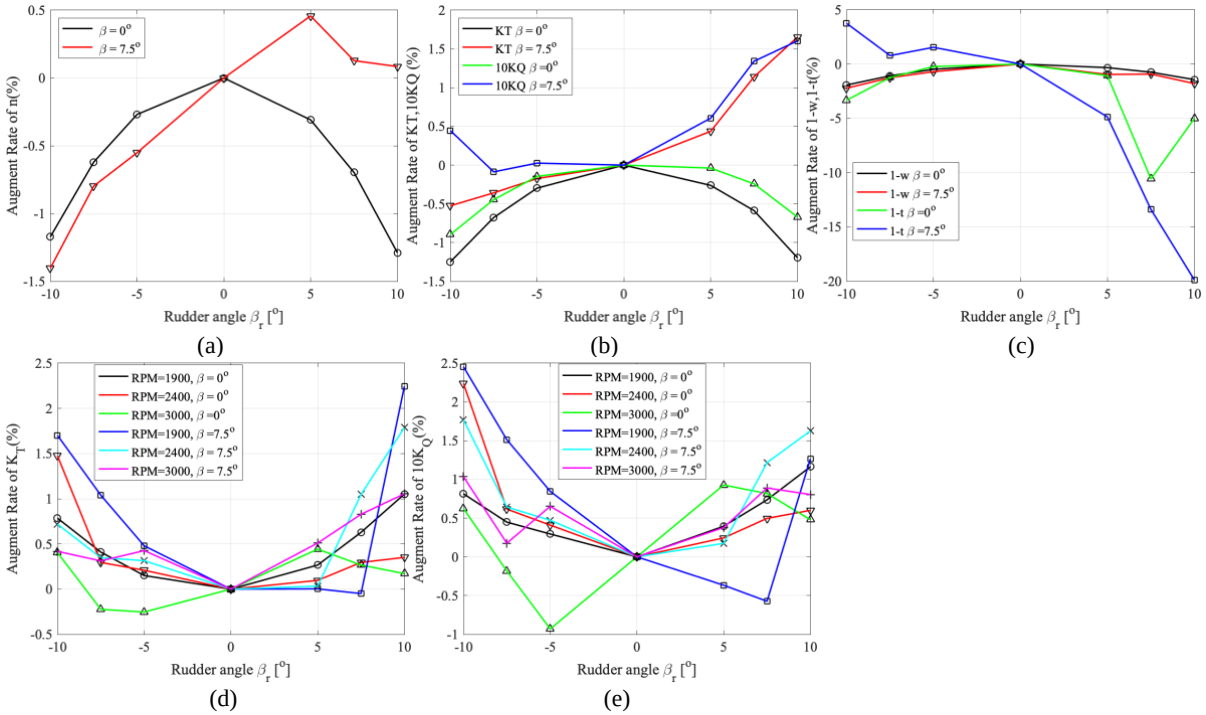


*Figure 4. Influence of drift angle on propulsive performance.*

**Propulsive performance**

Following the ITTC 1978 performance prediction approach, the propulsive characteristics of the self-propulsion and fixed RPM cases are presented in Figure 4. The augment rate is defined as Equation (5)

$$Augment\ rate\ (\%) = \frac{(A_n - A_0)}{A_0} \times 100 \quad (5)$$

Where $A_0$ is the value for 0° rudder angle in each scenario, used as a benchmarking point. $A_n$ is arbitrary point, n is the rudder angle annotation and n ranges from -10 to +10.

Variation in the rotation rate n in the self-propulsion test is shown in Figure 4 (a), where the augment rate is negative for all rudder angles when drift is 0° and the plot is axisymmetric around the $\beta_r$=0° line. The rudder angle farther from 0° exhibit a more evident decrement in the rotation rate. When 7.5° drift is applied to the KCS, the augment rate is positive for positive rudder angles while it is negative for negative rudder angles. The maximum difference is between $n_{-10}$ and $n_5$, about 2 %.

The coefficients of thrust and torque for the self-propulsion tests are shown in Figure 4 (b). When the hull has zero drift angle, both the maximum thrust and torque can be observed at $\beta_r$=0°. The remaining cases with non-zero rudder angles follow similar tendency for thrust and torque: $K_{T\,-r}$= $K_{T\,+r}$ and $K_{Q\,-r}$= $K_{Q\,+r}$. However for the 7.5° drift cases, the thrust coefficient, augment rate is negative for negative $\beta_r$ while it is positive for positive $\beta_r$. In comparison, all torque coefficients have a positive augment for all non-zero rudder angles except for $\beta_r$=-7.5° whose augment rate is -0.1%. Variation of $K_T$ and $K_Q$ for fixed RPM cases are shown in Figure 4 (d) and (e) respectively. When $\beta$=0°, both thrust and torque coefficients have a positive augment for all $\beta_r$ in the fixed RPM 1900 and 2400 tests. The largest augment happens for RPM=1900 at $\beta_r$=+10° while for RPM=2400 it happens at $\beta_r$=-10°. For cases of RPM=3000, both plots of thrust and torque coefficients show central symmetry. The coefficients of -$\beta_r$ and +$\beta_r$ are almost equivalent, and the larger augment rate points occurs when $\beta_r$=-5° and +5°. For fixed RPM cases with 7.5° drifting, all thrust and torque coefficients have positive increment in addition to $\beta_r$=5° and 7.5° when RPM=1900. The largest increment rates are found for $K_T$ at $\beta_r$=10° while for $K_Q$ at $\beta_r$=-10°.

Furthermore, the plot of wake fraction and thrust deduction variation for all rudder angles is shown in Figure 4 (c). The wake fraction shows similar trends for both 0° and 7.5° drift: axisymmetric about $\beta_r$=0° and the augment rate is within 3% for all $\beta_r$. In terms of thrust deduction, the increment rate is all negative for 0° drifted case while positive for negative rudder angles and negative for positive rudder angles when $\beta$=7.5°. The biggest decrement rate is approximately 20% at $\beta_r$=10°.

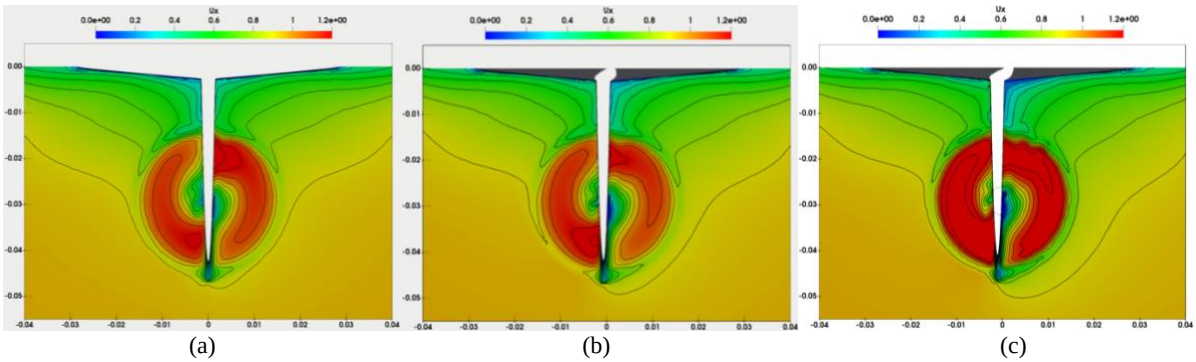

(a) (b) (c)

*Figure 5. Local axial flow (Ux) at x/Lpp=0.9911 at the angle of drift 0° with different rudder angles. (a) Rudder angle 0°, (b) Rudder angle 5°, (c) Rudder angle 7.5°.*

Figure 5 presents the axial velocity contours behind the propeller of the KCS for three different rudder angles. It is found that even a small increment of the rudder angle results in a more obviously asymmetric wake profile.

## 5 Conclusion and future work

This paper presents computations of the KCS with static drift angles and a series rudder angles in calm water. The computed results include resistance, lateral force, yaw moment, propulsive characteristics, and axial velocity, which provide some insight into hull-appendage interaction and allows for ship maneuvering studies. It is concluded that the method based on an OpenFOAM RANS solver with coupling to Blade Element Momentum theory can predict ship maneuvering performance in a reasonably accurate and cost-effective way. The capability of the RANS-BEMt propeller modelling approach for capturing hull-propeller-rudder interaction in drifting conditions has been demonstrated. Future investigations will include the influence of the free surface, and simulations in regular waves to better predict the self-propelled ship's maneuvering performance in more realistic conditions.

## Acknowledgement

The authors acknowledge the use of the IRIDIS5 High Performance Computing Facility, and associated support services provided by HPC team at the University of Southampton, in the completion of this work.

## References

Badoe, C.E., 2015. Design practice for the stern hull of a future twin-skeg ship using a high fidwlity numerical approach. University of Southampton. https://doi.org/10.1109/fie.2016.7757408

Badoe, C.E., Phillips, A.B., Turnock, S.R., 2015. Influence of drift angle on the computation of hull-propeller-rudder interaction. Ocean Eng. 103. https://doi.org/10.1016/j.oceaneng.2015.04.059

ITTC, 2021. The Specialist Committee on Manoeuvring in Waves - Final Report and Recommendations to the 29th ITTC.

Jiang, L., Yao, J., Liu, Z., 2022. Comparison between the RANS Simulations of Double-Body Flow and Water–Air Flow around a Ship in Static Drift and Circle Motions. J. Mar. Sci. Eng. 10. https://doi.org/10.3390/jmse10070970

Molland, A.F., Turnock, S.R., Hudson, D.A., 2017. Ship resistance and propulsion, Marine Propellers and Propulsion. https://doi.org/10.1016/B978-075068150-6/50014-0

OpenFOAMFoundation, 2019. OpenFOAM version 7 . URL https://openfoam.org/download/7-source/

Phillips, A.B., Turnock, S.R., Furlong, M., 2010. Accurate capture of propeller-rudder interaction using a coupled blade element momentum-RANS approach. Sh. Technol. Res. 57. https://doi.org/10.1179/str.2010.57.2.005

Phillips, A.B., Turnock, S.R., Furlong, M., 2009. Evaluation of manoeuvring coefficients of a self-propelled ship using a blade element momentum propeller model coupled to a Reynolds averaged Navier Stokes flow solver. Ocean Eng. https://doi.org/10.1016/j.oceaneng.2009.07.019

Sanada, Y., Park, S., Kim, D.H., Wang, Z., Stern, F., Yasukawa, H., 2021. Experimental and computational study of hull-propeller-rudder interaction for steady turning circles. Phys. Fluids 33. https://doi.org/10.1063/5.0073098

Turnock, S.R., Phillips, A.B., Furlong, M., 2008. URANS SIMULATIONS OF STATIC DRAFT AND DYNAMIC MANEUVERS OF THE KVLCC2 TANKER, in: Workshop on Verification and Validation of Ship Maneuvering Simulation Methods-SIMMAN 2008. Force Technology, Copenhagen, Denmark.

Windén, B., 2021. "An Open-Source Framework for Ship Performance CFD." 26th SNAME Offshore Symposium, Virtual, April 2021. doi: https://doi.org/10.5957/TOS-2021-22

Windén, B., 2021. Predicting the powering performance of different vessel types using an open-source CFD propulsion framework, in: SNAME Maritime Convention 2021, SMC 2021. https://doi.org/10.5957/SMC-2021-132

Windén, B., 2014. Powering Performance of a Self Propelled Ship in Waves. University of Southampton.

Zhang, Y., Hudson, D., Windén, B., Turnock, S., 2021. Evaluating the effects of drift angle on the self-propelled ship using Blade Element Momentum Theory, in: 23rd Numerical Towing Tank Symposium. Mülheim an der Ruhr, Germany.